Journal of Zhejiang University-SCIENCE A (Applied Physics & Engineering)
ISSN 1673-565X (Print); ISSN 1862-1775 (Online)
www.jzus.zju.edu.cn; link.springer.com
E-mail: jzus_a@zju.edu.cn

On the role of hemodynamics in predicting rupture of the abdominal aortic aneurysm

Maria Antonietta BONIFORTI†, Lorenzo DI BELLA, Roberto MAGINI

Department of Civil, Building, and Environmental Engineering, Sapienza University, Rome 00184, Italy

†E-mail: antonietta.boniforti@uniroma1.it

Received July 3, 2021; Revision accepted Sept. 17, 2021; Crosschecked Nov. 18, 2021

Abstract: Hemodynamics plays a crucial role in the growth of an abdominal aortic aneurysm (AAA) and its possible rupture. Due to the serious consequences that arise from the aneurysm rupture, the ability to predict its evolution and the need for surgery are of primary importance in the medical field. Furthermore, the presence of intraluminal thrombus (ILT) strongly affects the evolution of the pathology. In this study, we analyzed the influence of hemodynamics on the growth and possible rupture of AAAs. Numerical investigations of pulsatile non-Newtonian blood flow were performed in six patient-specific AAAs reconstructed from diagnostic images, having different sizes and shapes, and with or without ILT. Wall shear stress and vorticity distribution in the bulge and their evolution during the cardiac cycle were analyzed. The results indicate that blood flow dynamics acts synergistically with atherosclerotic degeneration in the development of the disease. The high surface complexity and tortuosity of the aneurysms significantly affect the blood motion, and the presence of inflection in the aneurysm centerline has a noticeable effect on the vortex dynamics. Links between regions of slow recirculating flows, low values of time-averaged wall shear stress, high values of oscillatory shear index, and zones of ILT deposition were found. In the absence of ILT, possible thrombus accumulation areas and consequent aneurysm growth were identified. The findings of this study highlight the importance of hemodynamics in assessing the vulnerability of the aortic wall and underline the crucial role of patient-specific investigations in predicting the rupture of individual aneurysms.

Key words: Hemodynamics; Computational fluid dynamics; Wall shear stress; Vortex dynamics; Abdominal aortic aneurysm (AAA); Patient-specific modelling

https://doi.org/10.1631/jzus.A2100308 **CLC number:** O351.2; R732.21

1 Introduction

An abdominal aortic aneurysm (AAA) is a dilation of the aortic wall localized between the renal arteries and the iliac bifurcation. An aortic dilatation is considered an aneurysm when it involves an increase in diameter above 50% with respect to the diameter of a healthy aorta, which is about 2.0 cm in the abdomen (Gopalakrishnan et al., 2014; Kent, 2014).

Factors reducing aortic wall integrity and increasing the risk of rupture include wall asymmetry, heterogeneity, and low compliance of the wall. When the stress on the aneurysm wall exceeds the wall strength, the dilated artery ruptures, causing a hemorrhage which is frequently lethal. From a medical point of view, even today, the size of the aneurysm is considered the best predictor of this dramatic event. While the size and shape of a healthy aorta do not change much in different subjects, there are large variations in aneurysm geometry, and therefore large differences in the shear stress to which the arterial wall is subjected (Gasser et al., 2010; Xenos et al., 2010). These stresses are larger than those of a healthy aorta, due to the different sizes, shapes, and

ORCID: Maria Antonietta BONIFORTI, https://orcid.org/0000-0002-8221-2650

stiffnesses of the aneurysm. Nevertheless, non-homogeneity of the aneurysmal wall implies changes at the local tissue level that alter the mechanical properties and the thickness of the wall as the aneurysm progresses. This suggests that AAA wall strength is not related only to the maximum transverse diameter (di Martino et al., 2006). Confirming this, findings from clinical trials and autopsies have shown both the rupture of small/medium AAAs and the perfect integrity of large AAAs over long periods (Darling et al., 1977; Nicholls et al., 1998; Vorp, 2007; Gopalakrishnan et al., 2014; Huang et al., 2016; Laine et al., 2016; Haller et al., 2018). This makes the choice of surgery more difficult for physicians, as the risk of the repair is also high (Lasheras, 2007), and shows that the maximum diameter of the aneurysm cannot be the only indicator of the probability of rupture.

Therefore, it is necessary to consider not only anatomical indications, but also hemodynamic factors that act synergistically with atherosclerotic degeneration in the development of the disease and in the associated risk of rupture, to predict the rupture of the aneurysm and plan surgery.

Significant but controversial effects on aneurysmal pathology can be produced by the presence of intraluminal thrombus (ILT). Most AAAs, especially the larger ones, have a thrombus between the external aortic wall and the lumen, which is the region where the blood flows (Li and Kleinstreuer, 2007; Doyle et al., 2014). An ILT is an accumulation of fibrin, blood cells, platelets, blood proteins, and cellular debris adhering to the AAA inner wall. It is commonly found in most AAAs and it is associated with the progression of the disease. In particular, ILT was observed near the site of rupture in 80% of autopsies (da Silva et al., 2000), and was often associated with local hypoxia and wall weakening (Vorp et al., 2001). Moreover, the wall underlying ILT is thinner than the wall exposed to blood, and shows signs of inflammation and proteolytic degradation (Vorp et al., 2001; Swedenborg and Eriksson, 2006).

The causes of ILT, the ways in which it grows and the role it plays in the evolution of the disease are important elements under study. The mechanism leading to ILT formation is complex and not fully understood. According to some studies, platelets subjected to high shear stress are activated and aggregate. Due to the recirculation motion inside the aneurysm, they become trapped in a vortex ring, which carries them in its propagation from the proximal to the distal end of the aneurysm. The platelets are then released during the break up of the vortex and adhere to regions with low shear stress where they enter into contact with the susceptible endothelium, thus initiating the formation of a thrombus (Bluestein et al., 1996; Lasheras, 2007; Biasetti et al., 2010; di Achille et al., 2014; Bhagavan et al., 2018).

Once an ILT is deposited, it is likely that a further accumulation process is favored in the same place. In most cases, the thrombus covers only some areas of the aneurysm where there are signs of elastic degradation and inflammation, and where the underlying wall is thinner than that without ILT deposition (Swedenborg and Eriksson, 2006). Both the presence of ILT and its thickness influence aneurysm growth (Vorp et al., 2001; Kazi et al., 2003; Swedenborg and Eriksson, 2006; Li et al., 2008; Qiu et al., 2019; Zhu et al., 2020). Several researchers reported that the presence of ILT reduces peak wall stress in abdominal aneurysms, with a beneficial effect against rupture (Wang et al., 2002; Li et al., 2008; Georgakarakos et al., 2009). Despite these results, the presence of a thrombus appears overall to be negative, because the ILT-covered wall is thinner than the surrounding wall, and rich in inflammatory cells (Kazi et al., 2003). Recently, the presence of ILT has been associated with early rupture of small AAAs, although they have shown a reduced peak wall stress (Haller et al., 2018; Qiu et al., 2019). In fact, the protective effect that ILT can furnish by reducing the stress on the artery wall is sometimes canceled by the weakening of the vessel wall produced by thrombus deposition (Speelman et al., 2010). Therefore, ILT accumulation can be considered as an index of high-risk of rupture for small aneurysms (Haller et al., 2018) and a predictor of AAA growth (Zhu et al., 2020).

Wall shear stress (WSS) on the lumen wall plays an important role in the development of an aneurysm, its eventual rupture, and the formation of any thrombus. The non-physiological values that occur during the cardiac cycle contribute to the degradation of the wall and the progression of AAA. Recently, simulating steady blood flows in realistic geometries of rupted AAAs, Boyd et al. (2016) found that rupture

occurs at regions of flow recirculation, where low WSS and thrombus deposition predominate. Differently, in unsteady blood flows, which characterize AAAs, low time-averaged wall shear stress (TAWSS) and recirculating blood flow have been suggested as being responsible for the deterioration of the arterial wall (Cecchi et al., 2011; Tarbell et al., 2014; Kelsey et al., 2017; Takehara et al., 2020). In unsteady blood flow, a high oscillatory shear index (OSI) has also been recognized as inducing an inflammatory response (Sorescu et al., 2004). The role of WSS was investigated by Scardulla et al. (2017) in relation to the use of a left ventricular assist device to treat advanced cardiac heart failure.

Thus, while unidirectional shear stress is associated with a healthy state, regions characterized by low WSS and high OSI are susceptible to thrombus formation and consequently to a higher risk of aneurysm rupture. Furthermore, compared to healthy aorta values, lower WSS and higher OSI values have been found in the aneurysm dilatation (Takehara et al., 2020), and the altered non-physiologic shear stress was indicated to promote the growth and possible rupture of the aneurysm (Cecchi et al., 2011).

In particular, low values of WSS are associated with a negative effect on the normal physiology of the endothelial cells and may contribute to local remodeling of the vessel wall, and aneurysm growth and rupture. Recent findings confirmed that endothelial cells exposed to low WSS with variable direction are activated and show inflammation (Gijsen et al., 2019). Non-physiologic low WSS with a high OSI characterizes the flow field in AAA, as shown also by a recent in vivo assessment with 4D-flow magnetic resonance imaging (MRI) (Takehara et al., 2020). Moreover, the low-velocity blood flow inside an aneurysm results in an increased residence time of the blood circulating particles near the aneurysm wall, thus extending their interactions with vascular endo-
[illegible]
particles have prolonged contact with the wall and their adhesion is inversely related to the WSS (Hinds et al., 2001). In addition, the complex and asymmetrical geometries of the abdominal aneurysms determine the complex distributions of the WSS in space and time. The development and consequences of this pathology are peculiar to each patient and underline the need for a patient-specific hemodynamic analysis. Despite the influence of the numerous factors previously described, it seems reasonable to think that the AAA rupture can occur in areas with recirculation and low WSS and where ILT accumulated, in which the wall could be particularly weak (Wolf et al., 1994; Stenbaek et al., 2000; Kazi et al., 2003; Koole et al., 2013; Qiu et al., 2019).

To provide physicians with more complete and reliable indicators to describe the progression of the aortic disease, this study highlights how computational fluid dynamics can represent a fundamental diagnostic support tool for predicting the evolution of the disease and supporting its treatment (Pasta et al., 2017). The understanding of the phenomena associated with local hemodynamics, the evaluation of WSS, and the analysis of the complex interactions between blood flow and inflammatory processes of the artery wall are crucial in assessing the possibility of aneurysm rupture. However, the unsteady nature of the pulsating flow, the particular rheological properties of blood, as well as the presence of macro vortices, make the analysis of the hemodynamic field extremely complex. Some considerations on the hemodynamics in AAAs with patient-specific geometry are presented, analyzing the influence of geometry, tortuosity, and the presence of ILT to identify areas of possible rupture of the aneurysm wall. Numerical simulations of blood flow in physiological conditions of pulsating motion were carried out in six different AAAs characterized by the presence of a thin (<5 mm) or thick (>5 mm) thrombus. The factors that can influence the development and possible rupture of the aneurysmal dilatation were analyzed, highlighting similarities and differences among the various cases. In particular, 2D streamlines on suitable longitudinal cross-sections, as well as WSS and vorticity distributions in the bulge, were determined throughout the cardiac cycle. Of particular interest was the analysis of the spatial distributions of hemodynamic quantities averaged over the cardiac cycle, such as time-averaged velocity, TAWSS, and OSI, which allows the identification of any areas that could be subject to rupture.

This paper is organized as follows. Firstly, the methods and setting up of the study are presented. In particular, the procedure for the 3D reconstruction of the aneurysms from computed tomography (CT)

images is described, and indications for the numerical investigation are provided. The main results obtained from the computational investigation of the hemodynamics in pulsatile and non-Newtonian blood flow conditions in the various aneurysms are then presented, with the aim of providing an understanding of the blood flow in the AAAs and predicting rupture. In particular, the spatial and temporal distributions of the flow pattern and the WSS in the patient-specific geometries are analyzed and their association with the presence of ILT and the potential vascular rupture are discussed. Finally, based on the fluid dynamics parameters examined and comparisons with recent literature, information is provided on the possible regions of ILT formation and on the determination of the areas in which AAA rupture could occur. The results presented contribute to the understanding of AAA biomechanics and the prediction of AAA rupture to aid clinicians in planning the treatment of AAAs.

2 Methods

2.1 Patient-specific model reconstruction

Patient-specific flow dynamics simulations can provide valuable information on the evolution of aneurysmal pathology and its associated risk of potential rupture. The first step in simulating blood flow in realistic geometries is the reconstruction of patient-specific models from a set of medical images, acquired by an available imaging technique such as MRI or CT. Since the image segmentation process provides the fluid domain to be used in the numerical simulations, it is crucial to perform this step correctly.

Six anonymous patient-specific AAAs, differing in terms of shape, dimensions of the enlargement, and presence of ILT, were analyzed. For each case, a set of images in DICOM (digital imaging and communications in medicine) format were acquired from CT scans and used for 3D reconstructions. The individual cases and the method of reconstruction of the patient-specific geometries are illustrated below.

First, using the open-source medical imaging acquisition ITK-SNAP software (v.3.8.0), a segmentation process was performed to convert 2D slices into 3D geometric models suitable for use in computational analysis. In ITK-SNAP the segmentation process involves several steps: (a) “snake”, i.e. identification of the anatomical region of interest; (b) “threshold”, i.e. adjustment of contrast values to highlight the aortic lumen, which is the area of the aneurysm affected by blood; (c) “bubbles radius and iterations”, i.e. definition of the contour of the selected aortic segment. All the patient-specific geometries were reconstructed from a section of the aorta from just below the renal arteries to the first part of the iliac bifurcation. From the segmentation process, a coarse 3D geometry of the AAA was obtained, showing regions with irregular and rough edges.

To smooth the rough surface of the models, further pre-processing was necessary. For this purpose, the Meshmixer 3.5 software (Autodesk, Inc., San Rafael, California, USA) was used to better delineate the aneurysmal area (“Sculpt”), cut the arterial branches (“Separate”), and close the areas of the eliminated arterial branches (“Autorepair”). Using this tool, visceral arteries and other minor arteries that branch off the aorta were occluded and the blood flow was confined to the aorta.

Subsequently, the open-source software Vascular Modeling Tool Kit (VMTK, version 1.4.0) made it possible to further smooth the surface and add cylindrical “flow extensions” to each model at the inlet and outlets. The role of the extensions was to lengthen the inflow and outflow zones to allow for flow development before affecting aneurysmal dilatation, and to mitigate boundary effects on numerical results. In all cases, the lumen volume was cut below the iliac bifurcation and minor branches of the aorta were occluded. Once the preliminary processing of medical images was completed, the specific geometry of each aneurysm was ready to be used for numerical investigations in STL format. The patient-specific models considered differed in the presence of curvature, neck angle (roughly, the angle between the neck axis and the centerline of the aneurysm in the initial region of the enlargement), bulge asymmetry, and ILT.

The STL files obtained for each aneurysm from the segmentation process were imported into ANSYS SpaceClaim (ANSYS Inc., 2020 R2), which allowed the extraction of surfaces from the STL files. This step consists in covering the entire surface of the 3D models with a “skin” that defines the surface of the

geometries to be used in the subsequent numerical investigations. The procedure required particular care to avoid errors that would alter the hemodynamic field, and was carefully performed for all six examined cases.

All the processes illustrated above were performed twice for the aneurysms characterized by the presence of a thrombus >5 mm thick: once considering only the lumen region, and once including the thrombus too. The two reconstructions were then superimposed for analyzing the cross-interactions between the hemodynamic field and the ILT. Segmentation of thin-layer ILT (thickness≤5 mm) was not performed because the boundaries could not be easily distinguished in CT images. For numerical fluid dynamics investigation of blood flow, only the lumen is obviously important, but the discussion and the concluding remarks take into account the link between the hemodynamic fields and the presence and position of the intraluminal thrombus.

The six patient-specific AAAs were classified into two groups, based on the thickness of the ILT. The first group (class A) included the aneurysms that did not have ILT or that had a very thin ILT (<5 mm). The second group included AAAs with ILT thickness of >5 mm (class B). There were two cases belonging to class A (aneurysms A1, A2) and four belonging to class B (aneurysms B1, B2, B3, B4). As previously mentioned, for all AAAs belonging to class B (>5 mm) two reconstruction processes were performed, one including the ILT region, and one with only the area affected by the blood flow (lumen). Fig. 1 shows the VMTK models obtained from the reconstruction procedure for all examined cases, and a rendering of the final geometries of the lumen.

2.2 Governing equations and numerical setup

Blood fluid dynamics in AAAs is difficult to simulate accurately because the flow is pulsating, blood is a non-Newtonian fluid, and the real geometries are extremely complex.

Taking this into account, numerical simulations were performed under pulsatile flow conditions, modeling blood as an incompressible non-Newtonian fluid with a dynamic viscosity μ=0.0035 kg/(m·s) and density ρ=1060 kg/m^3, and using the representative vascular geometries obtained from the segmentation process.

The mass and momentum conservation equations for an incompressible fluid and negligible gravity force are:

$$\nabla \cdot \boldsymbol{u} = 0, \tag{1}$$

$$\rho\left(\frac{\partial \boldsymbol{u}}{\partial t} + \boldsymbol{u} \cdot \nabla \boldsymbol{u}\right) = -\nabla p + \nabla \cdot \boldsymbol{\tau}, \tag{2}$$

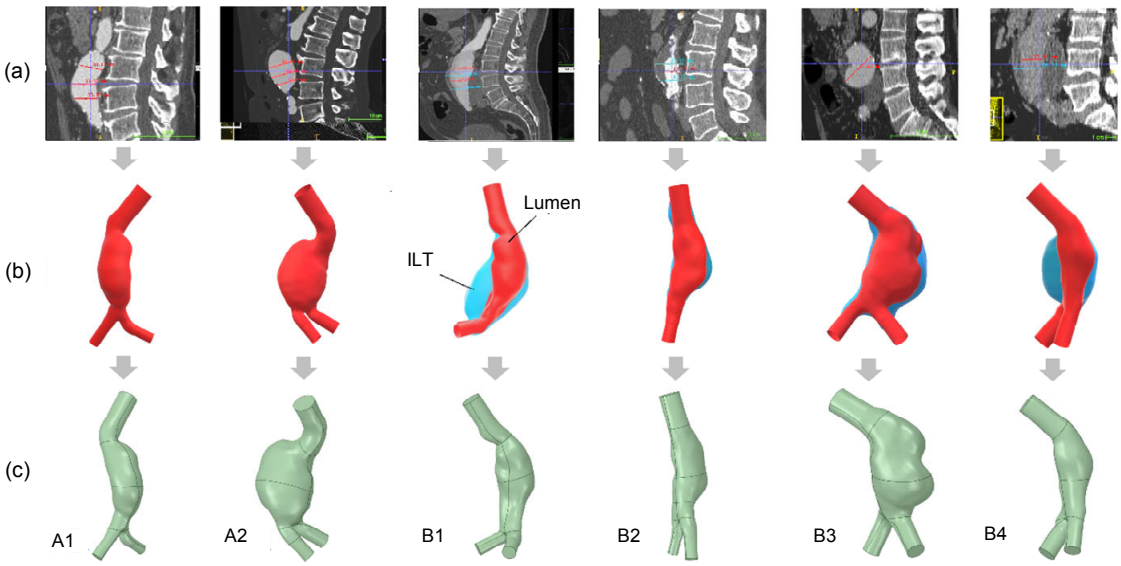

Fig. 1 Main steps of patient-specific aneurysm model reconstruction: (a) CT slices; (b) VMTK models; (c) final lumen geometries

where $\boldsymbol{u}$ is the velocity vector, t is the time, p is the pressure, and ρ is the density of the fluid. The deviatoric stress tensor $\boldsymbol{\tau}$ is a function of the strain rate tensor $\boldsymbol{D}$, according to the relation $\boldsymbol{\tau}=2\mu(\dot{\gamma})\boldsymbol{D}$, where μ is the dynamic viscosity of the fluid, $\dot{\gamma}$ is the shear rate, and $\boldsymbol{D}=(\nabla\boldsymbol{u}+\nabla\boldsymbol{u}^{\mathrm{T}})/2$.

The numerical investigations were performed using the commercial computational fluid dynamics software ANSYS Fluent (2020 R2). The transient formulations were performed under a 1st-order implicit method, the "semi-implicit method for pressure-linked equations" (SIMPLE) was used as pressure-velocity coupling algorithm, and a 2nd-order upwind scheme was adjusted for the spatial discretization of momentum equations. For setting up the simulations, the following basic assumptions were made. Firstly, as widely accepted in recent literature (Soudah et al., 2013; Lozowy et al., 2017; Patel et al., 2017; Qiu et al., 2019), the abdominal aneurysm wall was assumed to be rigid, due to the fact that AAAs become stiffer with the progression of the disease. Two more basic assumptions were the no-slip condition at the vascular wall and the laminar flow condition.

For the examined cases, the mean and maximum Reynolds numbers $Re=\rho UD/\mu$, calculated with the diameter D of the healthy aorta, the blood density ρ and dynamic viscosity μ, and the mean and maximum velocities U respectively, are shown in Table 1.

Table 1 shows that throughout the cardiac cycle the Reynolds number maintains values below 2300, which is the threshold for transition to turbulence in steady pipe flow, when Poiseuille's law holds. However, in this study, unsteady flow conditions of a non-Newtonian fluid are considered. Thus, the laminar flow condition is only an assumption, as often used in the literature (Zambrano et al., 2016; Kelsey et al., 2017; Qiu et al., 2019).

A realistic flow simulation in AAAs must consider the complex rheological properties of blood, which exhibits non-Newtonian behavior due to both its composition of suspended cells and the ability of red blood cells to deform and aggregate. In this study, the shear-thinning behavior of blood was approximated using the Carreau rheological model in which the dynamic viscosity varies according to the law:

$$\mu(\dot{\gamma})=\mu_{\infty}+(\mu_0-\mu_{\infty})\left[1+(\lambda\dot{\gamma})^2\right]^{\frac{n-1}{2}}, \tag{3}$$

where μ_0=0.056 kg/(m·s) is the viscosity at zero shear rate $\dot{\gamma}$, μ_{∞}=0.0035 kg/(m·s) is the viscosity for an infinite shear rate, λ=3.313 s is the relaxation time, and n=0.3568 is the power-law index (Shibeshi and Collins, 2005).

The unsteady pulsatile nature of the blood flow was modelled by assigning appropriate physiological boundary conditions. For the AAAs considered in this study, the velocity and pressure waveforms were not available. Therefore, typical velocity and pressure pulses of the abdominal aortic segment were used. A flat velocity profile $v(t)$, i.e. constant along the radial direction, was assigned as the inlet boundary condition, and a physiological pressure waveform $p(t)$ was prescribed at the outlet boundaries of the patient-specific models (Fig. 2). At the inlet section of the models, the peak systolic velocity of 0.3 m/s occurred at t=0.25 s, and a reverse flow velocity of −0.05 m/s, corresponding to the diastolic minimum, was observed at t=0.51 s. The flow and pressure waveforms were derived from Xenos et al. (2010).

The time step used for numerical integration was 0.005 s, two hundred times smaller than the period of the cardiac cycle, which was 1 s. A maximum of 200 iterations were performed for each time step. The

Table 1 Mean Reynolds number and maximum Reynolds number for each of the examined aneurysms

Aneurysm	Inlet diameter D (m)	Mean Reynolds number	Maximum Reynolds number
A1	0.020	536	1827
A2	0.018	482	1644
B1	0.025	670	2283
B2	0.017	456	1553
B3	0.022	590	2009
B4	0.019	509	1735

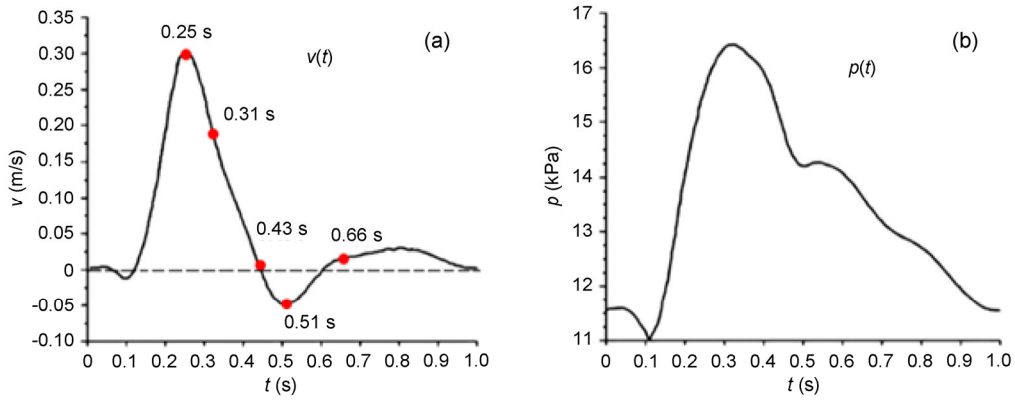

Fig. 2 Pulsatile velocity waveform prescribed at the inlet (a) and pressure waveform assigned at the outlet (b). The selected instants of the cardiac cycle are shown in the velocity waveform

threshold value for velocity components and continuity residuals was set as 10^{-5}. Three pulsatile cycles were simulated, but only the third cycle was analyzed, to minimize the influence of initialization effects. For the numerical flow simulations, different meshes were considered, with a refinement near the wall to capture the high velocity gradients in that area.

Obtaining mesh-independent solutions is a fundamental requirement for in-depth investigations of AAA hemodynamics, as the number of mesh elements can greatly affect the accuracy of the solutions. Mesh independency analysis was performed by monitoring the spatial average value of TAWSS to ensure that computational results were not sensitive to the mesh size. The final mesh volume was about 3 million elements for each model, which corresponds to an element size ranging from 0.35 mm for the smallest geometries to 0.60 mm for the largest.

To describe the flow field obtained from the numerical investigations, 2D and 3D streamline evolutions were analyzed, as well as the instantaneous WSS contours. Moreover, hemodynamic indicators, including TAWSS and OSI, were calculated to describe the unsteady nature of blood flow in the diseased arteries. TAWSS measures the magnitude of the WSS vector averaged over the cardiac cycle, whereas OSI takes into account changes in the direction of the WSS vector with respect to the dominant direction of the flow during the cardiac cycle. They are defined as follows (Ku et al., 1985):

$$\mathrm{TAWSS}=\frac{1}{T}\int_0^T|\mathbf{WSS}|, \tag{4}$$

$$\mathrm{OSI}=\frac{1}{2}\left(1-\frac{\left|\int_0^T \mathbf{WSS}\,\mathrm{d}t\right|}{\int_0^T|\mathbf{WSS}|\,\mathrm{d}t}\right), \tag{5}$$

where T is the period of the cardiac cycle, and **WSS** indicates the instantaneous WSS vector.

Finally, the evolution of vortical structures was analyzed, since development of vortices and slow circulation regions have been often associated with thrombus deposition and consequent weakening of the artery wall. The vortex core regions in the flow were identified by the Q-criterion method. The Q-criterion defines a vortex as a flow region with a positive second invariant of $\nabla \boldsymbol{u}$ (i.e. Q>0), and a lower pressure than the ambient value. A positive Q indicates that the rotation rate dominates the strain rate locally, so positive Q isosurfaces isolate regions occupied by vortices (Hunt et al., 1988). Thus, for an incompressible flow, Q represents the local balance between shear strain rate and rotation rate, and vortices coincide with areas where the magnitude of the vorticity is greater than the magnitude of the strain rate.

The results of the numerical investigations were analyzed over the entire cardiac cycle, and thus the considered time interval was [0 s, 1 s]. However, the numerical results are shown only at selected instants of the cardiac cycle considered significant for the evolution of the hemodynamic field (Fig. 2). In particular, they refer to the following phases of the cardiac cycle: the systolic peak at the instant characterized by maximum velocity at the inlet (t=0.25 s),

systolic deceleration (t=0.31 s and t=0.43 s), diastolic minimum (t=0.51 s), and diastolic acceleration (t=0.66 s). These instants are sufficient to capture the main peculiarities of streamline evolution, but the evolution of vortices is much more sensitive to time. Therefore, two more instants, t=0.10 s and t=1.00 s, were considered when describing the evolution of large vortex cores.

3 Results and discussion

Numerical simulations of the hemodynamic field within the six models of abdominal aneurysms with patient-specific geometry were performed under pulsatile flow conditions. A common feature of these aneurysms was the absence of symmetry. The asymmetrical expansion of a bulge is caused by the mechanical constraint in the posterior area because of proximity to the spinal column. The geometry of the considered aneurysms exhibited high surface complexity and significant tortuosity, particularly in the proximal and distal ends, which significantly affect the blood motion.

The blood flow into the aneurysms was analyzed to evaluate the flow patterns and WSS evolution during the cardiac cycle. Although it has been shown that under steady flow conditions a low WSS predominates at sites of AAA rupture (Boyd et al., 2016), more attention and additional hemodynamic indicators are necessary to describe the interaction between the pulsatile physiological blood flow and the artery wall. To quantify this interaction, the TAWSS and OSI were calculated for all patient-specific aneurysms. Moreover, the isosurfaces of the Q-criterion obtained by the numerical simulations were used to locate vortex core regions in the flow and display their evolution.

The flow characteristics at the selected time instants of the cardiac cycle were determined and compared across all cases. Particular attention was paid to the analysis of the spatial and temporal distributions of WSS, since low and oscillating WSS generated by the pulsatile motion seems to be associated with possible rupture of the aneurysm (Doyle et al., 2014; Boyd et al., 2016; Forneris et al., 2020). Moreover, low WSS values associated with high OSI values were found to promote inflammatory processes via the induced oxidative response in the endothelial vascular cells (Chatzizisis et al., 2007; Tarbell et al., 2014).

The results of the numerical simulations at the representative phases of the cardiac cycle are illustrated in the following. In particular, for each patient-specific model, a suitable cross-section of the aneurysm able to capture the maximum area in the longitudinal direction inside the lumen was identified. In this cross-section, the analysis of the evolution of 2D streamlines during the cardiac cycle allowed clarification of how the flow patterns and recirculation regions develop in time. The fluent option, "start from equally spaced samples" on the selected cross-section, was used to generate the 2D streamlines. In all the following figures, for the class B aneurysms, the portion of the 3D thrombus that would have obscured the view of the motion was made transparent.

Residual vortices emerging from the previous cycle were visible within the aneurysmal dilatation of all patient-specific models during the systolic acceleration phase of each cardiac cycle, as will be better described later by visualizing vortex core evolution during the cardiac cycle. These vortices were swept out of the aneurysm as the systolic peak approached (t=0.25 s), a condition in which no significant recirculation regions were observed (Figs. 3 and 4). At this instant, the WSS values were on average higher than in other instants of the cycle for all models, as described below.

At t=0.31 s, in the phase of systolic deceleration, a reverse flow near the proximal neck was observed, associated with small recirculation zones that gradually widened, but which showed reduced velocity in the subsequent phases of the cardiac cycle. This behavior was magnified for the aneurysm model A2 (Fig. 3). In this case, the sudden and significant widening of the vessel led to a consistent deceleration of the flow and an increase in pressure, determining the separation of the flow already at this instant.

As expected, a large counter-clockwise vortex formed in the anterior side for case A2, in which the maximum expansion occurred (Fig. 5) (p.967). Obviously, similar considerations were applied to all remaining patient-specific geometries, except for the B2 case where no significant tortuosity or neck angle was present.

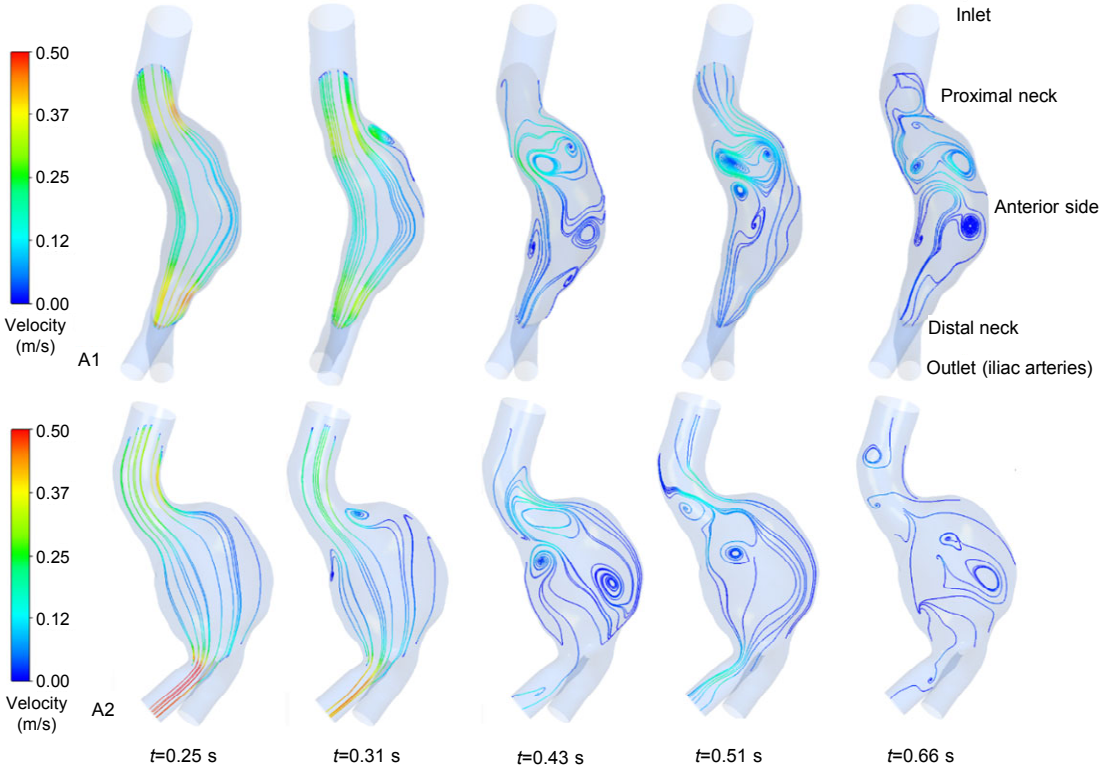

Fig. 3 2D streamlines on the longitudinal cross-sections of the patient-specific aneurysms A1 and A2

In the aneurysm B1, the ILT in the posterior region of the neck determined a non-physiological obstruction. As a result, separation of the flow and generation of a recirculation region had already taken place at this time (t=0.31 s).

At the end of the systolic phase (t=0.43 s), the velocity of the cardiac cycle prescribed at the numerical model inlet reached zero for all cases. Consequently, the flow field was strongly disturbed, a large number of new vortices arose, and the size of the pre-existing recirculation areas significantly increased, affecting the entire aneurysmal bulge. As previously observed, boundary layer separation with appearance of recirculating flow was favored both by a significant neck angle and a remarkable enlargement of the lumen. Specifically, the neck angle affected the position and extension of the recirculation: the larger the neck angle, the greater the recirculation. Unlike the other cases, the B2 model had a peculiar shape, because of the absence of neck and outlet angle and the presence of the bulge on only one side. As a consequence, the larger recirculation was located in the anterior dilated area, close to the bulge inlet. Nevertheless, the vanishing of the inlet velocity resulted in a large number of small vortices near the posterior wall of the aneurysm. In all remaining cases, recirculation areas affected the whole volume of the lumen, resulting in a complex flow that interacted with the endothelium.

At t=0.43 s, the vortex dynamics was particularly interesting in the case A2. At this instant, Fig. 3 shows that, in this aneurysm, the vortex in the anterior region of the proximal neck moved backward towards the healthy vessel, inducing enlargement of the small counter-rotating vortex located on the opposite posterior wall. Large recirculation regions spread over the entire lumen. This complex flow pattern correlates with the complexity of the A2 geometry that, in addition to tortuosity, highlights remarkable inflection points. In this regard, it is useful to recall the definition of tortuosity proposed by Soudah et al. (2013), who defined the aneurysm tortuosity by means of an index comparing the length of the AAA centerline with the length of a hypothetical healthy aorta. According to this definition, tortuosity does not necessarily imply inflection in the centerline of the

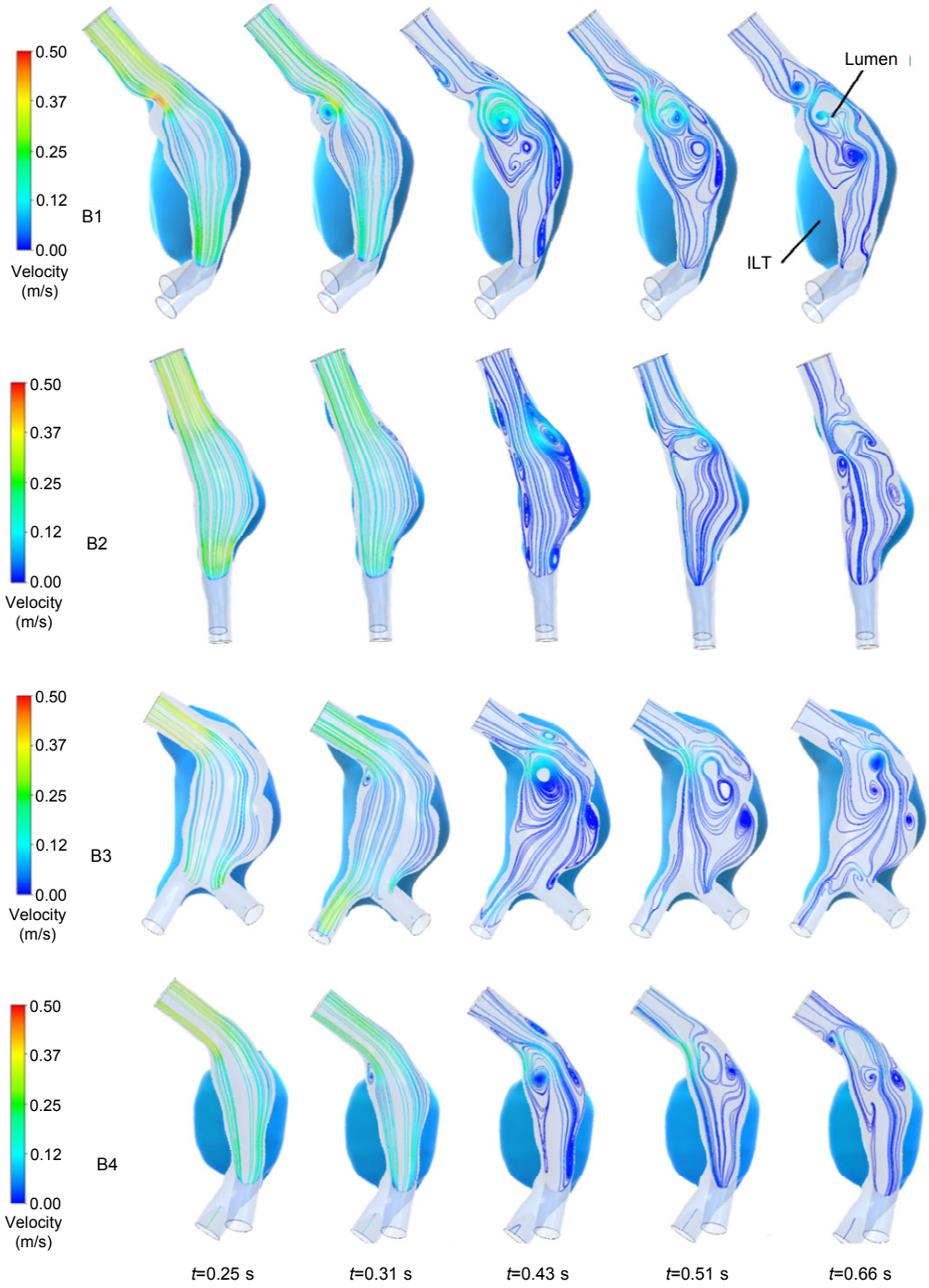

Fig. 4 2D streamlines on the longitudinal cross-section for the patient-specific aneurysms B1, B2, B3, and B4

aneurysm. Unlike other cases, A1 and A2 models showed both tortuosity and significant inflection points between the aneurysm inlet and the bulge, where the surface curvature changes from concave to convex, which greatly affect the motion. The simultaneous presence of large tortuosity and inflection seems also to influence strongly the temporal evolution of vorticity within the bulge, as will be described below.

At t=0.51 s, corresponding to the diastolic minimum, the inlet velocity became negative and a reverse flow condition prevailed both in the aneurysm

dilatation and in the iliac arteries. This negative flow phase was characterized by interactions between the pre-existing recirculation regions and the retrograde flow, which caused a weakening of the larger vortices and the disappearance of the smaller ones close to the wall. This is particularly evident in case B2 where, due to the absence of curvature, the retrograde flow tended to drag away the small recirculation areas near the posterior wall. In most cases, the main vortical structures formed in the previous instants and located in the central area of the bulge persisted, even if with a different shape and position, while the small recirculation regions near the wall were damped (Figs. 3 and 4).

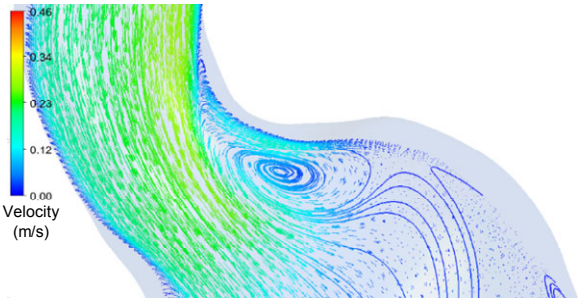

Fig. 5 Close-up of the streamlines and velocities in the neck region for the patient-specific aneurysm A2 (t=0.31 s)

This analysis of the spatial and temporal evolution of vortices during the cardiac cycle was based on examining the streamlines on the longitudinal cross-sections. However, there were also vortices at different levels of the transverse sections, associated with secondary flows. For a better understanding of the 3D vortex dynamics, the Q-criterion method was used. For example, Fig. 6 shows the 3D vortex core regions and the recirculation areas on the longitudinal plane for the A1 model at t=0.51 s. It is possible to observe how the 3D vortices obtained from the Q-criterion (magenta color) were correlated to the 2D flow on the longitudinal plane (dark gray color) previously defined. In particular, it can be seen how the vortex cores correspond with the center of the vortices highlighted by the 2D streamlines. In Fig. 6, the coherence between the results from streamlines and the Q-criterion is highlighted.

In the phase of diastolic acceleration, a weak reorganization of the previously disrupted flow could be observed. In contrast, in the last instants of the cycle, a large number of slow recirculation zones re-appeared as the velocity assigned on input tended to zero again. The flow subsequently became realigned during the systolic acceleration phase, and the process resumed identical to the previous cycle.

Additional information on the vortex dynamics was obtained by analyzing the temporal evolution of the vortex core isosurfaces, detected by the Q-criterion method. An appropriate threshold for visualizing these isosurfaces was selected to highlight the main vortex rings inside the patient-specific aneurysm. This value was the same for all examined AAAs to allow comparisons among the various cases. For the aneurysms A1 and A2, the area affected by the vortices progressively widened throughout the cardiac cycle, affecting the entire aneurysmal dilatation during late diastole (Fig. 7).

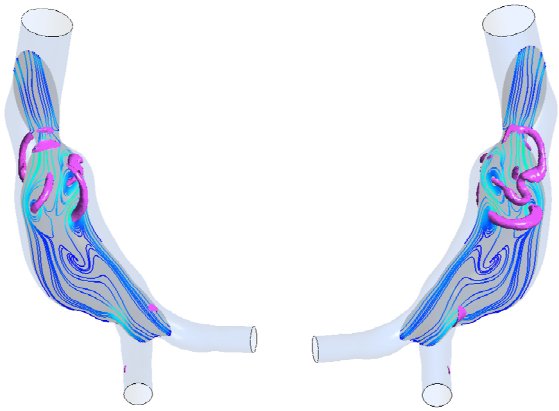

Fig. 6 2D streamlines on the longitudinal cross-section (dark gray color) and vortex core regions (magenta color) determined using the Q-criterion at t=0.51 s for the patient-specific aneurysm A1

It is interesting to note the peculiar vortex dynamics that characterize these aneurisms. For these cases, there are inflection points between the proximal neck and the bulge, where the surface curvature changes significantly from concave to convex. As a consequence, the vortex core region, initially located in the neck area, widened during the diastolic phase of the cardiac cycle, greatly affecting the aorta dilatation. Thus, a larger region of the aneurysmal bulge than in the other cases was affected by the main vortices. For the remaining aneurysms (cases B1, B2, B3, and B4), the main vorticity tended to remain more confined to the proximal neck area (Fig. 8) (p.969).

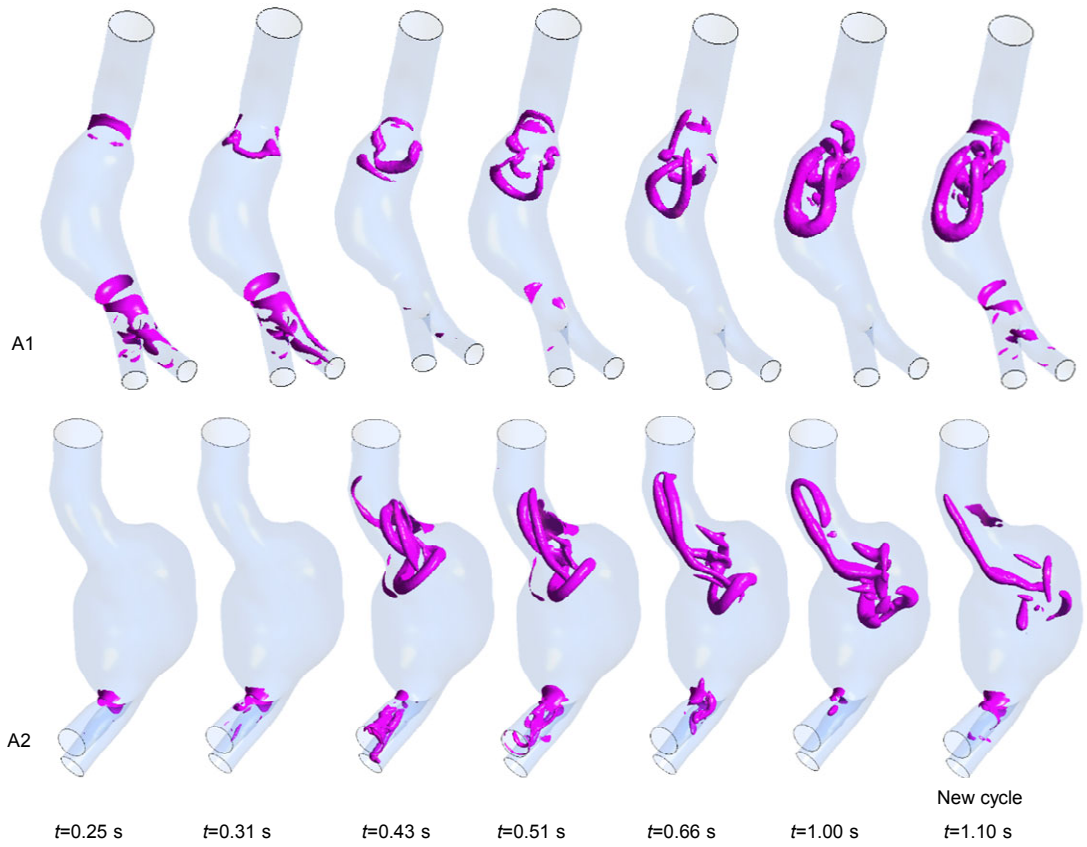

Fig. 7 Vortex core isosurfaces determined with the *Q*-criterion for the patient-specific aneurysms A1 and A2. Since the period of the cardiac cycle was equal to 1.00 s, the instant 0.10 s was replaced with 1.10 s for a continuous visualization of the vortex dynamics

For all cases, the *Q*-criterion enhanced the results of the 2D-streamline analysis, that is, each cardiac cycle inherited vortices from the previous cycle. Then, during the systolic acceleration phase, these vortices progressively disappeared as the systolic peak was reached, due to the action of the incoming accelerating flow.

Subsequently, the deceleration of the flow and the adverse pressure gradient determined by the enlarged diseased artery caused the onset of new vortex rings that progressively strengthened and occupied an increasingly wider region of the aneurysm. Such complex vortex dynamics gave rise to non-physiological WSS that in turn appeared to be negatively correlated with ILT accumulation (Kelsey et al., 2017; Tzirakis et al., 2017) and disruption of artery wall integrity (Koole et al., 2013).

In summary, for all examined patient-specific models, a similar behavior of vortex generation and propagation was observed during the cardiac cycle. The main vortex ring originates during the systolic deceleration phase (t=0.31 s) near the neck region, as a result of the detachment of the flow due to the enlargement of the section, which is associated with the presence of ILT in the neck in cases B1 and B3. The vortex area migrates towards the center of the aneurysm during the diastolic phase. Large recirculation regions, characterized by extremely low velocity values were observed when the inlet velocity was zero or close to zero (t=0.43 s, t=0.66 s, and t=1.00 s). Thereafter, the vortices decreased in number and size during the later phases of the cardiac cycle and gradually disappeared during the systolic acceleration phase. Several geometric factors affect the flow entering the bulge. The position of the recirculation areas depends on the specific geometry of the aneurysm, on its asymmetry and tortuosity, and on the neck angle, which influences the vorticity substantially.

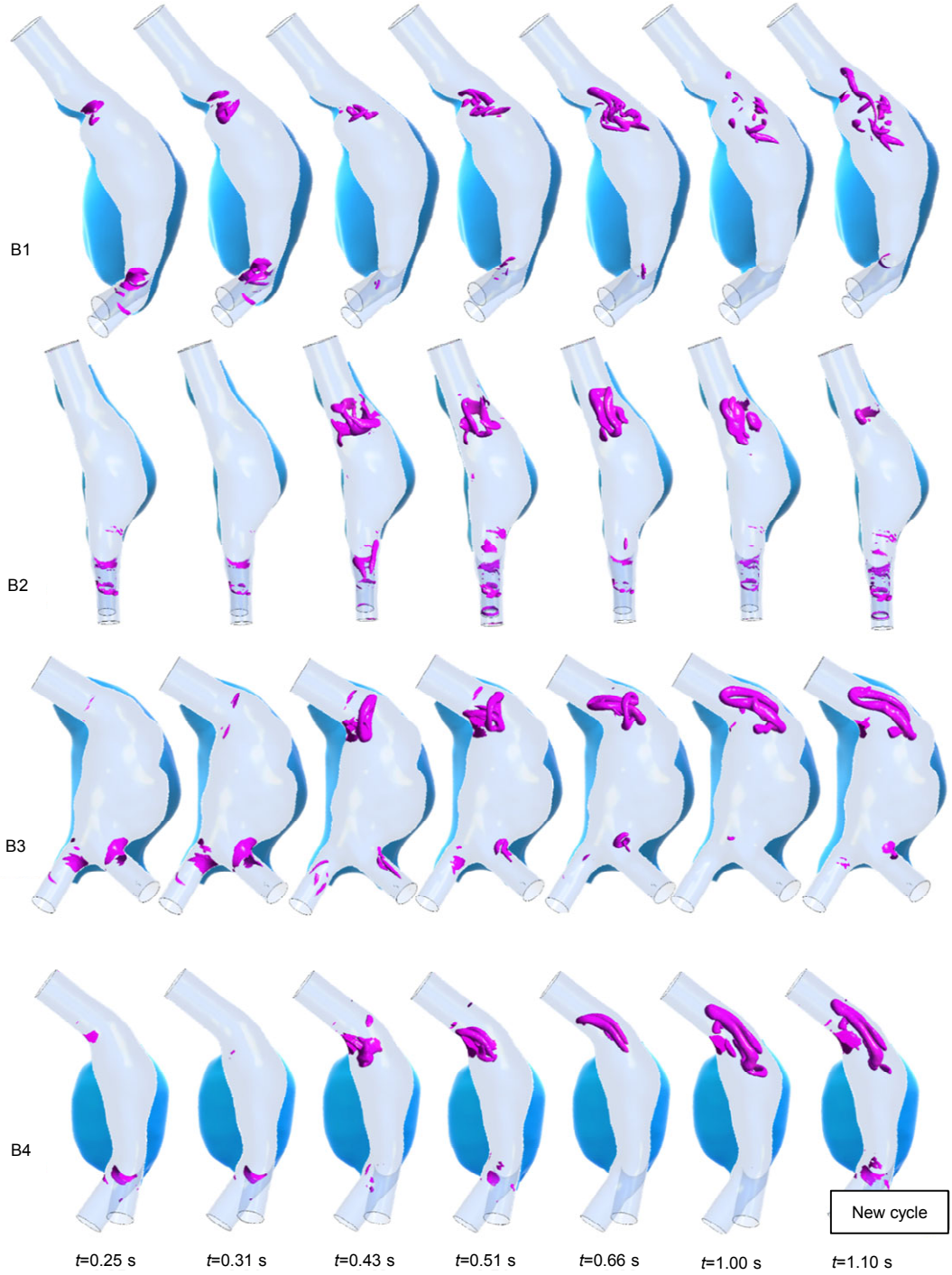

Fig. 8 Vortex core isosurfaces determined with the *Q*-criterion for the patient-specific aneurysms B1, B2, B3, and B4

Furthermore, the presence of inflection in the aneurysm centerline substantially affects the vortex dynamics, such as in the A1 and A2 models. In these cases, during the entire diastolic phase and the first instants of the systolic acceleration phase, the strongest vorticity regions spread over the entire bulge, while in the other cases they remained confined to the proximal neck areas.

The previous considerations are significant because the development of vortices and slow circulation

regions during the late systolic and the whole diastolic phases seems to be associated with thrombus deposition and consequent possible weakening of the wall. Platelets enveloped by the vortex rings can be activated as they enter the aneurysm (Bluestein et al., 1996; Biasetti et al., 2011). After, platelets tend to be deposited in areas of low shear stress, attaching themselves to pre-existing ILT or to the distal regions of the aneurysm. This is supported by the common occurrence of ILT in the distal anterior region of AAAs (Hans et al., 2005; Kelsey et al., 2017). In particular, using a fluid chemical model to predict ILT formation in abdominal aneurysms, Biasetti et al. (2012) showed a link between the motion of the vortical structures in the AAA and the clinical observations of the thickest ILT in the distal region. The presence of ILT can increase the risk of aneurysm rupture, since the aneurysm wall underlying the thrombus is thinner, contains fewer elastin fibers than a healthy wall, has many inflammatory cells, and shows signs of proteolytic degradation (Kazi et al., 2003). Nevertheless, it must be emphasized that while the presence of vortices can promote the formation of thrombus, the presence of ILT in turn contributes to the generation of vortices, so there is a close cross-link between these two factors.

3.1 Role of wall shear stress

As previously described, low TAWSS and recirculating flow have been suggested as being responsible for the deterioration of the arterial wall, and regions characterized by low WSS and high OSI are susceptible to thrombus formation and consequently to a higher risk of aneurysm rupture. According to these indications, in this study, recirculation regions characterized by low TAWSS and high OSI were considered to have the typical features of aneurysm rupture.

Fig. 9 shows the instantaneous WSS contours obtained from the numerical simulations. The temporal and spatial distributions of WSS values inside the AAA were found to depend on its specific geometry, which affects the observed flow separation and consequent emergence of recirculation regions. Thus, the shear stresses on the wall were found to differ from the physiological values of non-diseased arteries.

At the systolic peak (t=0.25 s) the WSS contour distributions show high values in the neck zone, where the curvature is high, and in the distal end of the aneurysmal sac, in proximity to the iliac arteries, for all patient-specific models. In agreement with the results of Soudah et al. (2013), who examined the flow at the instant of systolic peak, in the aneurysm bulge low-WSS regions coincided with low-velocity recirculation areas. High WSS values were found on the opposite side of the jet impingement, where the local neck curvature causes strong velocity gradients (Fig. 9a).

This behavior is particularly evident for all cases, except B2. Due to its specific geometry, in this case the angle of attack of the neck with respect to the aneurysm was almost zero and the direction of the main flow entering the sac was approximately "aligned" with the posterior wall. Therefore, there was no flow impingement, and the WSS in the proximal neck area was lower than in the other cases.

In summary, the presence of the neck angle is responsible for the generation of flow recirculation, inducing a sharp increase in WSS values within the inner bend of the neck. The location and size of this area depend on the curvature of each artery, in agreement with literature (Ku, 1997; Lasheras, 2007; Soudah et al., 2013). In Fig. 9a, the arrows indicate the neck regions that are associated with high WSS values due to the neck angle curvature. High WSS values were also found in the iliac arteries, generated by the tortuosity and narrowing of the vessels. Nevertheless, these areas, which are outside the aneurysmal dilatation, were not of interest to the present investigation.

During the systolic deceleration phase, the maximum WSS values in the aneurysm move towards the underlying areas, while remaining in the neck region (Fig. 9b). Nevertheless, the WSS maximum intensity decreases, as well as WSS values throughout the aneurysmal sac.

At t=0.43 s, again in the systolic deceleration phase, large areas of slow recirculation appear as a consequence of the zero inlet velocity and the WSS values decrease further (Fig. 9c). At the diastolic minimum, i.e. t=0.51 s, although associated with low velocities, the interactions between secondary flows and the retrograde flow led to local small increases in WSS, but no significant changes were detected on

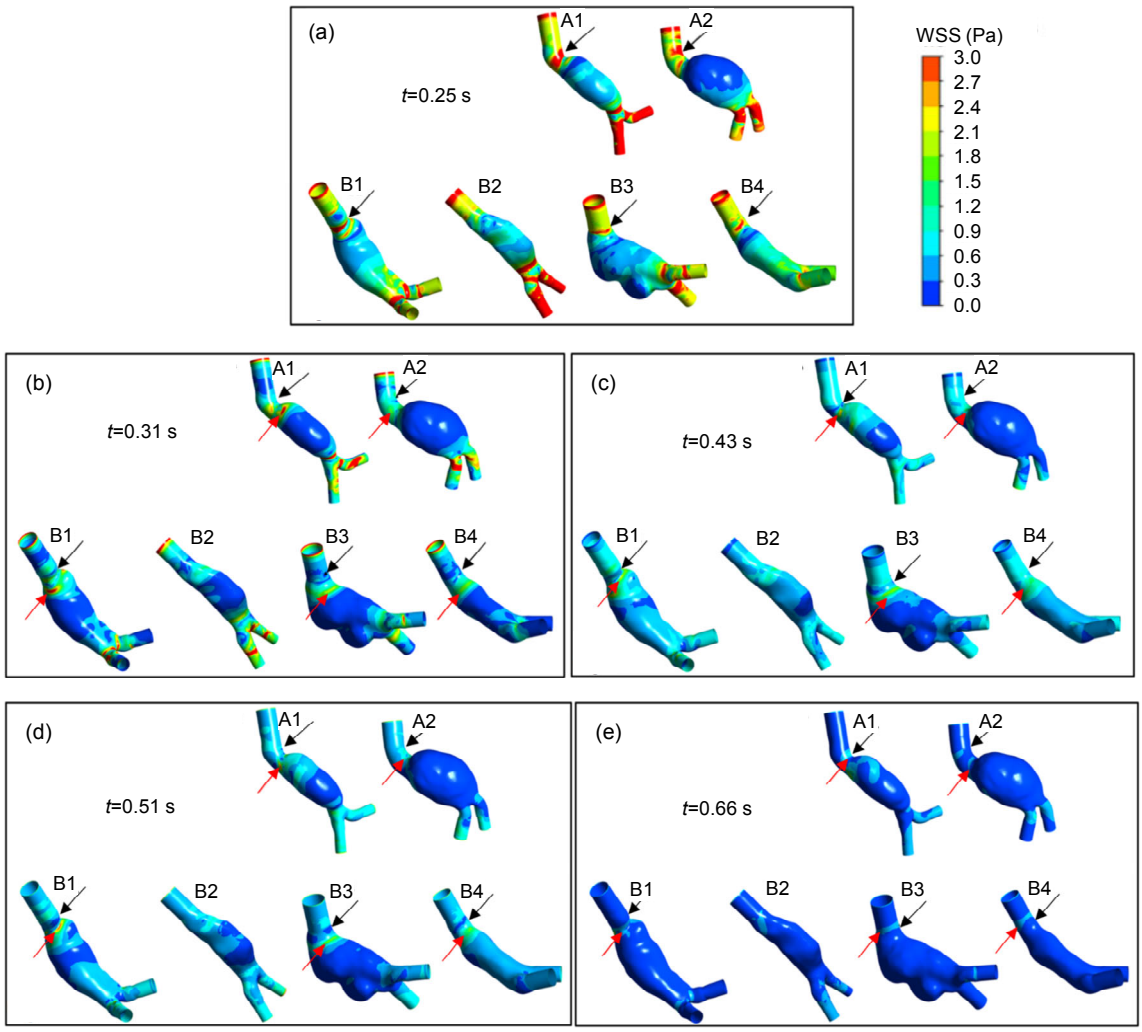

Fig. 9 WSS contour distribution at t=0.25 s (a), t=0.31 s (b), t=0.43 s (c), t=0.51 s (d), and t=0.66 s (e). Red arrows indicate the sites of high WSS. Black arrows indicate high WSS sites at the systolic peak instant (t=0.25 s)

average (Fig. 9d). Finally, at t=0.66 s, corresponding to the diastolic acceleration phase, the WSS values decreased drastically, but remained significant in the high-curvature areas of the neck (Fig. 9e).

As highlighted for the selected time instants, high WSS values are always associated with regions characterized by strong curvature throughout the cardiac cycle, such as the fold of the aneurysmal neck. In general, the instantaneous WSS values were low along the aneurysmal wall, but reached high values near the proximal and distal aneurysm sites, in agreement with published results (Soudah et al., 2013; Doyle et al., 2014; Boyd et al., 2016). The neck angle affected not only the vorticity field, but also the WSS distributions significantly.

3.2 Time-averaged hemodynamic indicators

Some additional hemodynamic quantities, averaged over the entire cardiac cycle, were evaluated to describe in detail the interaction between pulsating blood flow and the aneurismal wall. In particular, the space-time distributions of the WSS, provided by the numerical simulations, allowed to calculate the TAWSS and OSI. As previously seen, low WSS and high OSI induced an inflammatory and thrombotic state, leading to a deterioration of the arterial wall and consequently a higher risk of aneurysm rupture.

In this study, TAWSS and OSI were analyzed to understand the link between blood flow patterns, ILT accumulation, and the risk of aneurysm rupture for all

considered patient-specific aneurysms. In addition, contours of the time-averaged velocity fields on longitudinal cross-sections were examined. Finally, regions characterized by the presence of ILT were compared to the local behavior of the velocity field, TAWSS, and OSI. Fig. 10 illustrates the TAWSS, OSI, and time-averaged velocity contours for the aneurysms A1 and A2 in which ILT was absent or negligible (maximum thickness<5 mm). The same indicators are shown in Fig. 11 for the aneurysms belonging to class B, i.e. with a maximum ILT thickness of >5 mm. Results of the numerical simulations showed that low mean velocities were correlated with low TAWSS and high OSI for all cases

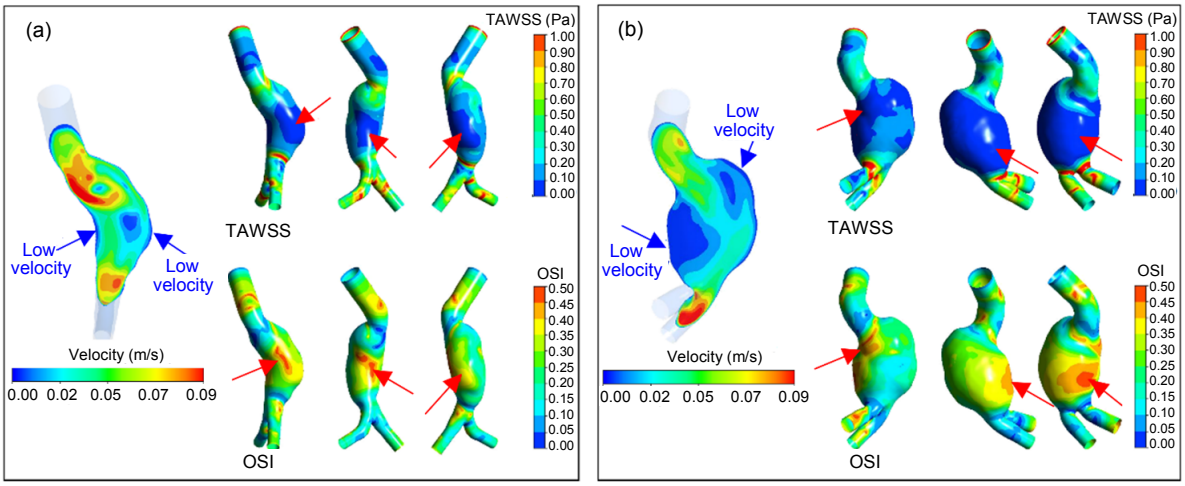

Fig. 10 Time-averaged velocity contours on the longitudinal cross-section and TAWSS and OSI on the luminal surfaces for the patient-specific aneurysms A1 (a) and A2 (b) (different views are shown). Red arrows indicate minimum TAWSS and maximum OSI; blue arrows indicate low velocity

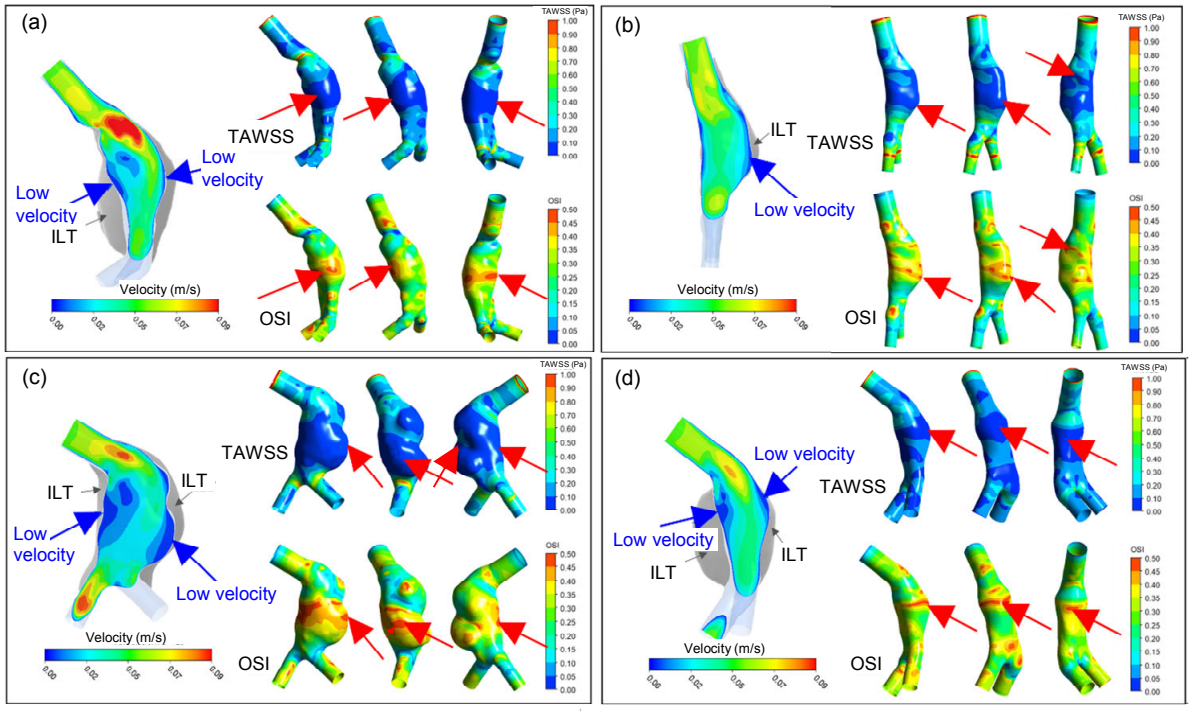

Fig. 11 Time-averaged velocity contours on the longitudinal cross-section and TAWSS and OSI on the luminal surfaces for the patient-specific aneurysms B1 (a), B2 (b), B3 (c), and B4 (d) (different views are shown). Red arrows indicate minimum TAWSS and maximum OSI; blue arrows indicate low velocity

(Figs. 10 and 11). Moreover, for the aneurysms B1, B2, B3, and B4, thrombus deposition was observed just in these areas, thus indicating a spatial correlation between flow stagnation regions, low and oscillating WSS, and presence of ILT (Fig. 11).

These results are in agreement with the published finding of low WSS in regions where ILT accumulated (Boyd et al., 2016; Zambrano et al., 2016; Kelsey et al., 2017; Lozowy et al., 2017), while high WSS could prevent thrombus formation. Furthermore, in recent studies which analyzed the association between AAA hemodynamic factors and thrombus growth, low TAWSS was observed in regions where the ILT subsequently accumulated. In particular, Zambrano et al. (2016) from a follow-up of 14 patients suggested that even the presence of a low TAWSS might promote ILT accumulation, and low time-averaged velocity regions coincided with those that experienced an ILT growth. Another recent longitudinal study revealed that high levels of ILT growth are associated with low TAWSS levels, and there is a positive association between OSI and ILT growth (Tzirakis et al., 2017).

Following this logic, as regards the A1 and A2 aneurysms characterized by the absence of ILT or the presence of very thin ILT, it is reasonable to hypothesize a possible further accumulation of ILT in the regions where the numerical investigation indicated low average velocities, low values of TAWSS, and high OSI values. As a result of this work, this consideration is of particular interest since most studies indicate an association between ILT and growth and early rupture of AAAs (Koole et al., 2013; Haller et al., 2018; Zhu et al., 2020). In fact, formation of thick-layered ILT prevents the flux of oxygen towards the aortic wall, causing local hypoxia, further thinning, and weakening of the adjacent wall (Vorp et al., 2001; Kazi et al., 2003; Swedenborg and Eriksson, 2006). Furthermore, comparing AAAs with and without ILT, Zambrano et al. (2016) showed that aneurysms with ILT exhibited lower values of WSS and higher values of AAA expansion, implying that low WSS may promote not only ILT accumulation, but also AAA growth. Besides ILT, recirculation regions and WSS values must be considered in aneurysm growth and rupture. Doyle et al. (2014) investigating an abdominal aneurysm from the time of detection to immediately prior to rupture, showed that AAA expansion and ILT accumulation coincided spatially with regions of low TAWSS, and rupture occurred in the low-TAWSS region, where the flow was recirculating. Confirming this, aneurysm rupture was recently observed at sites of reduced velocity, characterized by recirculation, low TAWSS, and thick thrombus deposition (Forneris et al., 2020).

The thickness of the ILT also needs to be considered. In general, in the presence of ILT, the largest abdominal aneurysms are those with the greatest accumulation of ILT. The maximum diameter (including thrombus) usually corresponds to the region of maximum thickness of the ILT (Koole et al., 2013; Tong et al., 2015; Zambrano et al., 2016). Although it is generally accepted that the presence of ILT is associated with AAA growth (Wolf et al., 1994; Kazi et al., 2003; Parr et al., 2011; Zhu et al., 2020), the thickness of the thrombus can also contribute to the growth and rupture of the aneurysm, due to its association with vascular cell apoptosis and degradation of elastin (Koole et al., 2013). Moreover, ILT thickness increases with increasing diameter of the AAA, while the lumen area seems to remain nearly constant (Zambrano et al., 2016). Therefore, the deposition of ILT increases the growth rate of the aneurysm. In the patient-specific aneurysms examined in this study, a greater maximum diameter was associated with a greater maximum thickness of the ILT, in agreement with literature (Koole et al., 2013; Tong et al., 2015; Zambrano et al., 2016).

The results of the numerical investigations indicated that the greater expansion of the aneurysms, including the thrombus regions, is not always localized in the area of main flow impingement. This was particularly evident in the cases of B1 and B4 patient-specific geometries, which exhibited extremely consistent ILT. A patient follow-up, which could have included an investigation of the history of thrombus accumulation in different stages of development of the pathology, was not available for the present study. Therefore, the above considerations refer only to the situation at the time of acquisition of the diagnostic images.

3.3 Study limitations

The findings of this study have to be seen in light of some limitations. The artery wall was assumed rigid, as widely accepted in recent literature (Soudah

et al., 2013; Lozowy et al., 2017; Patel et al., 2017; Qiu et al., 2019). This hypothesis is supported by the fact that AAAs become stiffer with the progression of the disease (Vande Geest et al., 2006; Vorp, 2007), and degradation of elastin together with an increase in collagen fibers of the aortic wall characterizes the development of the aneurysm (Thubrikar et al., 2001; Tong et al., 2015; Kolipaka et al., 2016). The elasticity of the arterial is taken into account in fluid structure interaction models, and some of these investigations indicate that a rigid wall assumption overestimates the WSS (Decorato et al., 2011; Bai and Zhu, 2019). However, these models could have some limitations for patient-specific AAA investigations, if some of the patient-specific parameters, e.g. thrombus properties or artery wall stiffness, are missing or uncertain, as they are difficult to obtain. In this case, to consider arterial elasticity could be useless. Nevertheless, in future studies, it might be of interest to consider the elasticity of blood vessels in the study of the earlier stages of the disease.

Regarding the boundary conditions, although appropriate physiological boundary conditions were assigned to model blood flow, only published velocity and pressure pulses of the abdominal aortic segment were used, as the patient-specific data were not available. Obviously, more accurate results could be achieved by using patient-specific velocity and pressure waveforms. Moreover, although recent imaging techniques, such as 4D MRI, have been shown to be effective in measuring blood flow, their current spatial resolution limits their applicability in calculating hemodynamic parameters and they also do not provide information on the pressure field (Canchi et al., 2015).

4 Conclusions

The objective of this study was to analyze the influence of hemodynamic factors on the growth and possible rupture of AAAs. Numerical investigations of pulsatile non-Newtonian blood flow were performed in six patient-specific AAAs reconstructed from diagnostic images, of different sizes and shapes, and characterized by the presence of thin (<5 mm) or thick (>5 mm) ILT. The patient-specific aneurysm geometries exhibited a high surface complexity and significant tortuosity, particularly at the proximal and distal ends. The choice of real patient-specific geometries instead of idealized models, the presence of ILT, and the assumption of the non-Newtonian Carreau rheological model, allowed an accurate representation of real physiological blood flow.

In the examined patient-specific aneurysms, larger maximum diameters, including ILT, were found to be associated with thicker ILT, which confirms recent findings that the larger the aneurysm, the higher the accumulation of thrombus (Koole et al., 2013; Tong et al., 2015; Zambrano et al., 2016).

The specific aneurysm configurations strongly affected the blood motion inside the bulges, and the WSS distribution. In particular, the position of recirculation areas depended on the aneurysm asymmetry and tortuosity. In all examined cases, the same behavior of vortex generation and propagation was observed. The presence of ILT, the neck angle, and the vessel curvature contributed to the generation of vortices and secondary flows, with consequent possible ILT accumulation. It must be emphasized that the presence of inflection points in the aneurysm centerline was found to influence the vortex dynamics in a significant way, as noted in the A1 and A2 patient-specific models.

In addition, the results of the numerical investigation showed that the largest expansion of the aneurysm, including the thrombus regions, was not always localized in the area where the main flow impacted the wall.

In agreement with recent studies, high WSS values were found in the proximal neck area of the bulge, while lower values characterized the interior region throughout the cardiac cycle.

In zones with low time-averaged velocities, low TAWSS values and high OSI values were observed. These regions correlated with ILT deposition zones, when ILT was found in the aneurysms. In the absence of ILT, or the presence of only a very thin ILT, a possible thrombus accumulation in these regions was supposed. To confirm this, recent literature findings indicate that the growth of ILT is associated with low TAWSS and high OSI values, and rupture occurs at sites of reduced velocity, low TAWSS, and thick ILT (Zambrano et al., 2016; Tzirakis et al., 2017). Based

on these findings and the current numerical results about the aneurysms characterized by an absence of ILT or the presence of only a very thin ILT (cases A1 and A2), ILT accumulation with consequent possible rupture was hypothesized in regions where the numerical investigation indicated low time-averaged velocities, low TAWSS values, and high OSI values. Despite the previously described limitations, this study contributes to knowledge of the mechanisms of aneurysm growth and the prediction of the risk of rupture. Moreover, it highlights the importance of hemodynamics in assessing the vulnerability of the aortic wall and indicates that computational investigation using patient-specific models is useful for understanding the individual pathology supporting the clinical management of AAA disease.

Contributors

Maria Antonietta BONIFORTI designed and supervised the research. Lorenzo DI BELLA reconstructed the patient-specific models from diagnostic images. Maria Antonietta BONIFORTI, Lorenzo DI BELLA, and Roberto MAGINI carried out the study. Maria Antonietta BONIFORTI and Roberto MAGINI revised and edited the final version of the manuscript.

Conflict of interest

Maria Antonietta BONIFORTI, Lorenzo DI BELLA, and Roberto MAGINI declare that they have no conflict of interest.

This article does not contain any studies with human subjects performed by any of the authors.

References

Bai ZD, Zhu LD, 2019. Simulation of blood flow past a distal arteriovenous-graft anastomosis at low Reynolds numbers. *Physics of Fluids*, 31(9):091902. https://doi.org/10.1063/1.5099635

Bhagavan D, di Achille P, Humphrey JD, 2018. Strongly coupled morphological features of aortic aneurysms drive intraluminal thrombus. *Scientific Reports*, 8(1):13273. https://doi.org/10.1038/s41598-018-31637-6

Biasetti J, Gasser TC, Auer M, et al., 2010. Hemodynamics of the normal aorta compared to fusiform and saccular abdominal aortic aneurysms with emphasis on a potential thrombus formation mechanism. *Annals of Biomedical Engineering*, 38(2):380-390. https://doi.org/10.1007/s10439-009-9843-6

Biasetti J, Hussain F, Gasser TC, 2011. Blood flow and coherent vortices in the normal and aneurysmatic aortas: a fluid dynamical approach to intra-luminal thrombus formation. *Journal of the Royal Society Interface*, 8(63):1449-1461. https://doi.org/10.1098/rsif.2011.0041

Biasetti J, Spazzini PG, Swedenborg J, et al., 2012. An integrated fluid-chemical model toward modeling the formation of intra-luminal thrombus in abdominal aortic aneurysms. *Frontiers in Physiology*, 3:266. https://doi.org/10.3389/fphys.2012.00266

Bluestein D, Niu L, Schoephoerster RT, et al., 1996. Steady flow in an aneurysm model: correlation between fluid dynamics and blood platelet deposition. *Journal of Biomechanical Engineering*, 118(3):280-286. https://doi.org/10.1115/1.2796008

Boyd AJ, Kuhn DCS, Lozowy RJ, et al., 2016. Low wall shear stress predominates at sites of abdominal aortic aneurysm rupture. *Journal of Vascular Surgery*, 63(6):1613-1619. https://doi.org/10.1016/j.jvs.2015.01.040

Canchi T, Kumar SD, Ng EYK, et al., 2015. A review of computational methods to predict the risk of rupture of abdominal aortic aneurysms. *BioMed Research International*, 2015:861627. https://doi.org/10.1155/2015/861627

Cecchi E, Giglioli C, Valente S, et al., 2011. Role of hemodynamic shear stress in cardiovascular disease. *Atherosclerosis*, 214(2):249-256. https://doi.org/10.1016/j.atherosclerosis.2010.09.008

Chatzizisis YS, Coskun AU, Jonas M, et al., 2007. Role of endothelial shear stress in the natural history of coronary atherosclerosis and vascular remodeling: molecular, cellular, and vascular behavior. *Journal of the American College of Cardiology*, 49(25):2379-2393. https://doi.org/10.1016/j.jacc.2007.02.059

da Silva ES, Rodrigues AJ, de Tolosa EMC, et al., 2000. Morphology and diameter of infrarenal aortic aneurysms: a prospective autopsy study. *Cardiovascular Surgery*, 8(7):526-532. https://doi.org/10.1016/S0967-2109(00)00060-0

Darling RC, Messina CR, Brewster DC, et al., 1977. Autopsy study of unoperated abdominal aortic aneurysms. The case for early resection. *Circulation*, 56(S3):II161-4.

Decorato I, Kharboutly Z, Legallais C, et al., 2011. Numerical study of the influence of wall compliance on the haemodynamics in a patient-specific arteriovenous fistula. *Computer Methods in Biomechanics and Biomedical Engineering*, 14(S1):121-123. https://doi.org/10.1080/10255842.2011.593762

di Achille P, Tellides G, Figueroa CA, et al., 2014. A haemodynamic predictor of intraluminal thrombus formation in abdominal aortic aneurysms. *Proceedings of the Royal Society A: Mathematical, Physical and Engineering Sciences*, 470(2172):20140163. https://doi.org/10.1098/rspa.2014.0163

di Martino ES, Bohra A, Vande Geest JP, et al., 2006. Biomechanical properties of ruptured versus electively repaired abdominal aortic aneurysm wall tissue. *Journal of Vascular Surgery*, 43(3):570-576. https://doi.org/10.1016/j.jvs.2005.10.072

Doyle BJ, McGloughlin TM, Kavanagh EG, et al., 2014. From detection to rupture: a serial computational fluid dynamics case study of a rapidly expanding, patient-specific, ruptured abdominal aortic aneurysm. *In*: Doyle B, Miller K, Wittek A, et al. (Eds.), Computational Biomechanics for Medicine: Fundamental Science and Patient-specific Applications. Springer, New York, USA, p.53-68. https://doi.org/10.1007/978-1-4939-0745-8_5

Forneris A, Marotti FB, Satriano A, et al., 2020. A novel combined fluid dynamic and strain analysis approach identified abdominal aortic aneurysm rupture. *Journal of Vascular Surgery Cases, Innovations and Techniques*, 6(2):172-176. https://doi.org/10.1016/j.jvscit.2020.01.014

Gasser TC, Auer M, Labruto F, 2010. Biomechanical rupture risk assessment of abdominal aortic aneurysms: model complexity versus predictability of finite element simulations. *European Journal of Vascular and Endovascular Surgery*, 40(2):176-185. https://doi.org/10.1016/j.ejvs.2010.04.003

Georgakarakos E, Ioannou CV, Volanis S, et al., 2009. The influence of intraluminal thrombus on abdominal aortic aneurysm wall stress. *International Angiology*, 28(4): 325-333. https://doi.org/10.1038/hr.2009.89

Gijsen F, Katagiri Y, Barlis P, et al., 2019. Expert recommendations on the assessment of wall shear stress in human coronary arteries: existing methodologies, technical considerations, and clinical applications. *European Heart Journal*, 40(41):3421-3433. https://doi.org/10.1093/eurheartj/ehz551

Gopalakrishnan SS, Pier B, Biesheuvel A, 2014. Dynamics of pulsatile flow through model abdominal aortic aneurysms. *Journal of Fluid Mechanics*, 758:150-179. https://doi.org/10.1017/jfm.2014.535

Haller SJ, Crawford JD, Courchaine KM, et al., 2018. Intraluminal thrombus is associated with early rupture of abdominal aortic aneurysm. *Journal of Vascular Surgery*, 67(4):1051-1058. https://doi.org/10.1016/j.jvs.2017.08.069

Hans SS, Jareunpoon O, Balasubramaniam M, et al., 2005. Size and location of thrombus in intact and ruptured abdominal aortic aneurysms. *Journal of Vascular Surgery*, 41(4):584-588. https://doi.org/10.1016/j.jvs.2005.01.004

Hinds MT, Park YJ, Jones SA, et al., 2001. Local hemodynamics affect monocytic cell adhesion to a three-dimensional flow model coated with E-selectin. *Journal of Biomechanics*, 34(1):95-103. https://doi.org/10.1016/s0021-9290(00)00139-1

Huang Y, Teng ZZ, Elkhawad M, et al., 2016. High structural stress and presence of intraluminal thrombus predict abdominal aortic aneurysm ^{18}F-FDG uptake. *Circulation: Cardiovascular Imaging*, 9(11):004656. https://doi.org/10.1161/CIRCIMAGING.116.004656

Hunt JCR, Wray AA, Moin P, 1988. Eddies, streams, and convergence zones in turbulent flows. Proceedings of the Summer Program.

Kazi M, Thyberg J, Religa P, et al., 2003. Influence of intraluminal thrombus on structural and cellular composition of abdominal aortic aneurysm wall. *Journal of Vascular Surgery*, 38(6):1283-1292. https://doi.org/10.1016/S0741-5214(03)00791-2

Kelsey LJ, Powell JT, Norman PE, et al., 2017. A comparison of hemodynamic metrics and intraluminal thrombus burden in a common iliac artery aneurysm. *International Journal for Numerical Methods in Biomedical Engineering*, 33(5):e2821. https://doi.org/10.1002/cnm.2821

Kent KC, 2014. Clinical practice. Abdominal aortic aneurysms. *The New England Journal of Medicine*, 371(22): 2101-2108. https://doi.org/10.1056/NEJMcp1401430

Kolipaka A, Illapani VSP, Kenyhercz W, et al., 2016. Quantification of abdominal aortic aneurysm stiffness using magnetic resonance elastography and its comparison to aneurysm diameter. *Journal of Vascular Surgery*, 64(4): 966-974. https://doi.org/10.1016/j.jvs.2016.03.426

Koole D, Zandvoort HJA, Schoneveld A, et al., 2013. Intraluminal abdominal aortic aneurysm thrombus is associated with disruption of wall integrity. *Journal of Vascular Surgery*, 57(1):77-83. https://doi.org/10.1016/j.jvs.2012.07.003

Ku DN, 1997. Blood flow in arteries. *Annual Review of Fluid Mechanics*, 29:399-434. https://doi.org/10.1146/annurev.fluid.29.1.399

Ku DN, Giddens DP, Zarins CK, et al., 1985. Pulsatile flow and atherosclerosis in the human carotid bifurcation. Positive correlation between plaque location and low oscillating shear stress. *Arteriosclerosis*, 5(3):293-302. https://doi.org/10.1161/01.atv.5.3.293

Laine MT, Vänttinen T, Kantonen I, et al., 2016. Rupture of abdominal aortic aneurysms in patients under screening age and elective repair threshold. *European Journal of Vascular and Endovascular Surgery*, 51(4):511-516. https://doi.org/10.1016/j.ejvs.2015.12.011

Lasheras JC, 2007. The biomechanics of arterial aneurysms. *Annual Review of Fluid Mechanics*, 39:293-319. https://doi.org/10.1146/annurev.fluid.39.050905.110128

Li ZH, Kleinstreuer C, 2007. A comparison between different asymmetric abdominal aortic aneurysm morphologies employing computational fluid-structure interaction analysis. *European Journal of Mechanics-B/Fluids*, 26(5):615-631. https://doi.org/10.1016/j.euromechflu.2007.03.003

Li ZY, U-King-Im J, Tang TY, et al., 2008. Impact of calcification and intraluminal thrombus on the computed wall stresses of abdominal aortic aneurysm. *Journal of Vascular Surgery*, 47(5):928-935.

https://doi.org/10.1016/j.jvs.2008.01.006

Lozowy RJ, Kuhn DCS, Ducas AA, et al., 2017. The relationship between pulsatile flow impingement and intraluminal thrombus deposition in abdominal aortic aneurysms. *Cardiovascular Engineering and Technology*, 8(1):57-69. https://doi.org/10.1007/s13239-016-0287-5

Nicholls SC, Gardner JB, Meissner MH, et al., 1998. Rupture in small abdominal aortic aneurysms. *Journal of Vascular Surgery*, 28(5):884-888. https://doi.org/10.1016/s0741-5214(98)70065-5

Parr A, McCann M, Bradshaw B, et al., 2011. Thrombus volume is associated with cardiovascular events and aneurysm growth in patients who have abdominal aortic aneurysms. *Journal of Vascular Surgery*, 53(1):28-35. https://doi.org/10.1016/j.jvs.2010.08.013

Pasta S, Gentile G, Raffa GM, et al., 2017. Three-dimensional parametric modeling of bicuspid aortopathy and comparison with computational flow predictions. *Artificial Organs*, 41(9):E92-E102. https://doi.org/10.1111/aor.12866

Patel S, Usmani AY, Muralidhar K, et al., 2017. Effect of aorto-iliac bifurcation and iliac stenosis on flow dynamics in an abdominal aortic aneurysm. *Fluid Dynamics Research*, 49(3):035513. https://doi.org/10.1088/1873-7005/aa6a6b

Qiu Y, Wang Y, Fan YB, et al., 2019. Role of intraluminal thrombus in abdominal aortic aneurysm ruptures: a hemodynamic point of view. *Medical Physics*, 46(9):4263-4275. https://doi.org/10.1002/mp.13658

Scardulla F, Pasta S, D'Acquisto L, et al., 2017. Shear stress alterations in the celiac trunk of patients with a continuous-flow left ventricular assist device as shown by in-silico and in-vitro flow analyses. *The Journal of Heart and Lung Transplantation*, 36(8):906-913. https://doi.org/10.1016/j.healun.2017.03.016

Shibeshi SS, Collins WE, 2005. The rheology of blood flow in a branched arterial system. *Applied Rheology*, 15(6):398-405. https://doi.org/10.1901/jaba.2005.15-398

Sorescu GP, Song HN, Tressel SL, et al., 2004. Bone morphogenic protein 4 produced in endothelial cells by oscillatory shear stress induces monocyte adhesion by stimulating reactive oxygen species production from a nox1-based NADPH oxidase. *Circulation Research*, 95(8):773-779. https://doi.org/10.1161/01.RES.0000145728.22878.45

Soudah E, Ng EYK, Loong TH, et al., 2013. CFD modelling of abdominal aortic aneurysm on hemodynamic loads using a realistic geometry with CT. *Computational and Mathematical Methods in Medicine*, 2013:472564. https://doi.org/10.1155/2013/472564

Speelman L, Schurink GWH, Bosboom EMH, et al., 2010. The mechanical role of thrombus on the growth rate of an abdominal aortic aneurysm. *Journal of Vascular Surgery*, 51(1):19-26. https://doi.org/10.1016/j.jvs.2009.08.075

Stenbaek J, Kalin B, Swedenborg J, 2000. Growth of thrombus may be a better predictor of rupture than diameter in patients with abdominal aortic aneurysms. *European Journal of Vascular and Endovascular Surgery*, 20(5):466-469. https://doi.org/10.1053/ejvs.2000.1217

Swedenborg J, Eriksson P, 2006. The intraluminal thrombus as a source of proteolytic activity. *Annals of the New York Academy of Sciences*, 1085(1):133-138. https://doi.org/10.1196/annals.1383.044

Takehara Y, Isoda H, Takahashi M, et al., 2020. Abnormal flow dynamics result in low wall shear stress and high oscillatory shear index in abdominal aortic dilatation: initial in vivo assessment with 4D-flow MRI. *Magnetic Resonance in Medical Sciences*, 19(3):235-246. https://doi.org/10.2463/mrms.mp.2019-0188

Tarbell JM, Shi ZD, Dunn J, et al., 2014. Fluid mechanics, arterial disease, and gene expression. *Annual Review of Fluid Mechanics*, 46:591-614. https://doi.org/10.1146/annurev-fluid-010313-141309

Thubrikar MJ, Labrosse M, Robicsek F, et al., 2001. Mechanical properties of abdominal aortic aneurysm wall. *Journal of Medical Engineering & Technology*, 25(4):133-142. https://doi.org/10.1080/03091900110057806

Tong J, Cohnert T, Holzapfel GA, 2015. Diameter-related variations of geometrical, mechanical, and mass fraction data in the anterior portion of abdominal aortic aneurysms. *European Journal of Vascular & Endovascular Surgery*, 49(3):262-270. https://doi.org/10.1016/j.ejvs.2014.12.009

Tzirakis K, Kamarianakis Y, Metaxa E, et al., 2017. A robust approach for exploring hemodynamics and thrombus growth associations in abdominal aortic aneurysms. *Medical & Biological Engineering & Computing*, 55(8):1493-1506. https://doi.org/10.1007/s11517-016-1610-x

Vande Geest JP, Sacks MS, Vorp DA, 2006. The effects of aneurysm on the biaxial mechanical behavior of human abdominal aorta. *Journal of Biomechanics*, 39(7):1324-1334. https://doi.org/10.1016/j.jbiomech.2005.03.003

Vorp DA, 2007. Biomechanics of abdominal aortic aneurysm. *Journal of Biomechanics*, 40(9):1887-1902. https://doi.org/10.1016/j.jbiomech.2006.09.003

Vorp DA, Lee PC, Wang DHJ, et al., 2001. Association of intraluminal thrombus in abdominal aortic aneurysm with local hypoxia and wall weakening. *Journal of Vascular Surgery*, 34(2):291-299. https://doi.org/10.1067/mva.2001.114813

Wang DHJ, Makaroun MS, Webster MW, et al., 2002. Effect of intraluminal thrombus on wall stress in patient-specific

models of abdominal aortic aneurysm. *Journal of Vascular Surgery*, 36(3):598-604. https://doi.org/10.1067/mva.2002.126087

Wolf YG, Thomas WS, Brennan FJ, et al., 1994. Computed tomography scanning findings associated with rapid expansion of abdominal aortic aneurysms. *Journal of Vascular Surgery*, 20(4):529-538. https://doi.org/10.1016/0741-5214(94)90277-1

Xenos M, Rambhia SH, Alemu Y, et al., 2010. Patient-based abdominal aortic aneurysm rupture risk prediction with fluid structure interaction modeling. *Annals of Biomedical Engineering*, 38(11):3323-3337. https://doi.org/10.1007/s10439-010-0094-3

Zambrano BA, Gharahi H, Lim CY, et al., 2016. Association of intraluminal thrombus, hemodynamic forces, and abdominal aortic aneurysm expansion using longitudinal CT images. *Annals of Biomedical Engineering*, 44(5):1502-1514. https://doi.org/10.1007/s10439-015-1461-x

Zhu CC, Leach JR, Wang YT, et al., 2020. Intraluminal thrombus predicts rapid growth of abdominal aortic aneurysms. *Radiology*, 294(3):707-713. https://doi.org/10.1148/radiol.2020191723